Soft Matter

Colloidal swimmers near curved and structured walls

Journal:	*Soft Matter*
Manuscript ID	SM-ART-07-2019-001432.R2
Article Type:	Paper
Date Submitted by the Author:	03-Sep-2019
Complete List of Authors:	Das, Shibananda; Columbia University, Cacciuto, Angelo; Columbia University, Department of Chemistry

Soft Matter

ARTICLE TYPE

Cite this: DOI: 00.0000/xxxxxxxxxx

Colloidal swimmers near curved and structured walls

S. Das,[a] and A. Cacciuto*[a]

Received Date
Accepted Date

DOI: 00.0000/xxxxxxxxxx

We present systematic numerical simulations to understand the behavior of colloidal swimmers near a wall. We extend previous theoretical calculations based on lubrication theory to include walls with arbitrary curvature, and show how to extract from simulations a set of parameters crucial to accurately estimate the leading hydrodynamic contributions associated to the curvature of a wall. Our results show explicitly how introducing curvature to the wall, not only affects the average incident angle the swimmer acquires when swimming near it, but it also leads to much broader angular distributions. This suggests an increasingly leading role of thermal fluctuations with curvature, which in turn results in significantly different motility of the swimmers. We also show how the backwards motion previously reported for pushers also extends to puller-like swimmers under the appropriate conditions. Finally, aiming at understanding the behavior of colloidal swimmers near a colloidal crystal, we also considered the case of a wall built from colloidal particles that are either free to rotate, representing a crystal held together by isotropic forces, or have their rotational degrees of freedom locked-in, representing a crystal held together by directional interactions. In both cases, we find that puller-like swimmers follow a stochastic run-and-tumble-like dynamics.

1 Introduction

Self-propelled particles have received a considerable attention during the last few years due to their relevance in biological systems as well as their inherent out-of-equilibrium nature which lends promise for the development of the next generation of smart, responsive materials[1–11]. A critical aspect of active systems is the way hydrodynamic forces mediate the mutual interactions between active components and how they behave in the proximity of large surfaces[12–19]. Of particular interest is the tendency of micro-swimmers to accumulate near surfaces[20–23], a behavior that is routinely observed in experiments of artificial colloidal swimmers[24–28]. Specifically, active colloids are known to align their axis of propulsion to a specific orientation when in contact with a flat, smooth surface. This is due to a combined effect of the local chemical reactions generating fluid velocity gradients around the particle surface (which are ultimately responsible for its locomotion), and the no-slip constraint imposed on the fluid by the wall[29–33].

Simple theoretical arguments have been proposed to understand this behavior, and depending on the self-propelling mechanism, i.e. the specific slip velocity profile of the fluid at the particle surface, they lead to different orientations of a particle propelling axis[30,34–38]. To each orientation corresponds a different dynamical state. For instance, when the propelling axis of the particle is overall oriented towards the surface, but forms a specific angle smaller than $\pi/2$ with the surface normal, a lateral sliding motion of the particle is observed (forward motion). Whenever the angle the propelling axis forms with the surface normal is slightly larger than $\pi/2$, the particle moves along the surface (parallel motion) while an effective attraction of hydrodynamic nature keeps it from escaping the surface.

Most of the works with active particles near a wall have involved flat surfaces with few exceptions where convex surfaces were also considered [39,40]. These studies were put forward to understand the trapping (orbiting) of active colloids in a matrix of large passive colloids or columnar structures[25–27,40].

In this paper we go one step further, and present comprehensive theoretical and numerical results to detail the behavior of a model colloidal swimmer near smooth surfaces of arbitrary curvature, and near colloidal crystals interfaces, i.e. structured walls presenting a periodic modulation. We use lubrication theory for our analytical calculations and employ the multi-particle collision dynamics (MPC) method to represent the fluid in our numerical simulations. One advantage of this numerical method is that it explicitly accounts for thermal fluctuations and allows us to evaluate the relative thermal stability of the different states acquired by the particles.

Our results indicate that the swimmer dynamics has a systematic dependence on the surface curvature and can be estimated by theoretical calculations accounting for near-field lubrication forces in combination with an approximate far-field-like contribution. We observe that under the appropriate conditions both

[a] Department of Chemistry, Columbia University, 3000 Broadway, New York, NY 10027
* ac2822@columbia.edu

pullers and pushers can develop a backward motion near a no-slip smooth wall and gain a detailed insight into the mechanism leading to this behavior. An analogous phenomenology was recently reported only for pushers in references[38,41]. Finally, we study how relaxing the no-slip boundary condition by adopting a colloidal-crystal surface, where each particle is free to rotate, alters the motion of the active colloid near it. This study is crucial to understand the behavior of binary mixtures of active and passive particles.

2 Numerical model

We describe an active colloid using a discrete particle swimmer model similar to the one implemented for passive spherical colloids in references[42] and[43].

In this model, a colloid consists of 60 point particles placed according to a C_{60} geometry and one at its center. Each point on the surface is connected to its three neighboring points and simultaneously to the center one via harmonic bonds of the form

$$U(r) = \frac{K}{2}(r - r_0)^2, \tag{1}$$

where r_0 is the mean distance between two neighboring point particles, and the spring constant, K, is chosen to be large enough so that bond-length fluctuations are insignificant.

The surrounding fluid is described via multi-particle collision dynamics (MPC), a particle-based mesoscopic simulation method that naturally captures the effect of both hydrodynamic interactions and thermal fluctuations[44–46]. The MPC fluid consists of point particles of mass m moving according to a dynamics which includes a ballistic streaming step and a stochastic collision step. In the streaming step, the position of i-th fluid particle is updated as

$$\boldsymbol{r}_i(t + \Delta t_c) = \boldsymbol{v}_i(t)\Delta t_c, \tag{2}$$

where v_i is the velocity of i-th particle and Δt_c is the collision time. In the subsequent collision step, all the particles in the system are sorted into cells of cubic lattice size a, and the particles within a cell exchange momenta locally via a stochastic process. We employ the angular-momentum conserving stochastic rotation dynamics (SRD+a) approach of MPC, where the particle velocity after the collision is given by

$$\boldsymbol{v}_i(t + \Delta t_c) = \boldsymbol{v}_{cm}(t) + \mathscr{R}(\alpha)\boldsymbol{v}_{i,c}(t) - \boldsymbol{r}_{i,c}(t + \Delta t_c)\times \left[m\boldsymbol{I}^{-1}\sum_{j\in cell}\{\boldsymbol{r}_{j,c}(t + \Delta t_c)\times(\boldsymbol{r}_{j,c} - \mathscr{R}(\alpha)\boldsymbol{v}_{j,c}(t))\}\right]. \tag{3}$$

Here, $\boldsymbol{v}_i(t)$ and $\boldsymbol{v}_i(t + \Delta t_c)$ are the velocities before and after collision respectively, $\mathscr{R}(\alpha)$ is the rotation matrix with rotation angle α, $\boldsymbol{v}_{cm}(t)$ is the center-of-mass velocity of the considered cell, $\boldsymbol{r}_{i,c} = \boldsymbol{r}_i - \boldsymbol{r}_{cm}$ is the particle position relative to the center-of-mass position of the cell, $\boldsymbol{I}$ is the moment-of-inertia tensor of the particles in the center-of-mass reference frame, and $\boldsymbol{v}_{i,c} = \boldsymbol{v}_i - \boldsymbol{v}_{cm}$. Galilean invariance is maintained via a random shift of the collision grid in every collision step.

The coupling between the embedded colloid and the MPC fluid is achieved by including the colloidal point particles in the collision step for the local momenta exchange. The center-of-mass velocity of the collision cell containing N_c fluid particles and N_p colloidal surface points is given by

$$\boldsymbol{v}_{cm}(t) = \frac{\sum_{i=1}^{N_c} m\boldsymbol{v}_i(t) + \sum_{k=1}^{N_p} M\boldsymbol{V}_k(t)}{mN_c + MN_p}, \tag{4}$$

where M is the mass of each colloidal surface point, and $\boldsymbol{V}_k$ is the velocity of the k-th one. No-slip boundary condition for the fluid particles near a surface is achieved with a bounce-back rule, where a fluid particle reverses its velocity from $\boldsymbol{v}_i$ to $-\boldsymbol{v}_i$ when it hits the wall. The temperature of the system is maintained at a desired value via a collision-cell level thermostat, referred to as Maxwell-Boltzmann scaling (MBS) method. This ensures that the simulated system is in the canonical ensemble[47,48].

Following earlier works of active rods[49], we adopt a discrete version of the squirmer model to enforce self-propulsion of our colloidal particles. In our model, each of the C_{60} points describing the colloidal surface carries an intrinsic velocity $v_s(\theta_i)$, where θ_i is the polar angle of that point taken with respect to the axis of propulsion of the particle. $v_s(\theta_i)$ is given a predefined functional form which defines the type of swimmer under consideration. As a result, a fluid particle in a cell containing one of the C_{60} points, picks up an additional velocity

$$\boldsymbol{v}_a = \frac{M}{N_c}\boldsymbol{v}_s(\theta_i). \tag{5}$$

In the standard squirmer model, $v_s(\theta) = (2/3)u_0\sin\theta(1 + \beta\cos\theta)$, where the squirming parameters u_0 and β are used to characterize the velocity and the type of swimmer (pusher, puller, or neutral) respectively[35–37,50]. Here, we also consider the surface slip velocity proposed by Zhen. et. al.[37], where the two hemispheres of a colloid have two distinct slip velocity v_1 and v_2 such that

$$\begin{aligned} v_s(\theta) &= v_1\sin\theta, \text{ for } \cos\theta \geq 0 \\ &= v_2\sin\theta, \text{ for } \cos\theta < 0. \end{aligned} \tag{6}$$

This velocity profile provides a more realistic description of an active Janus colloidal particle where the two hemispheres have different material properties and correspondingly two different slip velocities and a discontinuity between the two. The swimming parameters in this case are given by[37]

$$u_0 = \frac{1}{3}(v_1 + v_2), \quad \beta = \frac{1}{2u_0}(v_1 - v_2). \tag{7}$$

The sum of all the slip momenta of the fluid particles are applied to the colloidal center of mass in the opposite direction such that the overall momentum is locally conserved over the length of colloidal swimmer body. The coupling between the fluid and the colloidal surface points in the collision step happens through the thermal velocities only, i.e., $\boldsymbol{V}_k(t)$ in Eq. 4 is the thermal contribution to the velocity of the colloidal surface points, while $\boldsymbol{v}_i(t)$ plays the same role as $\boldsymbol{V}_k(t)$, but for the fluid particles. Thus, no net external forces or torques act on the colloid.

When considering a flat, cylindrical or toroidal surface, an active colloid experiences a repulsive force due to a WCA-like po-

tential of the form

$$U(d_i^w) = 4\varepsilon\left[\left(\frac{\sigma}{d_i^w}\right)^{48} - \left(\frac{\sigma}{d_i^w}\right)^{24} + \frac{1}{4}\right]. \quad (8)$$

Here, d_i^w is the shortest distance between the particle and the wall. This potential extends up to $d_i^w = 2^{1/24}\sigma$.

In our simulations, all lengths are scaled by the collision-cell size a, masses by the fluid mass m, and energies by k_BT. Thus, the MPC time unit is $\tau = \sqrt{ma^2/k_BT}$. The MPC collision angle is set to $\alpha = 130°$, the collision time is $\Delta t_c = 0.05\tau$ and the average number of fluid particles per cell is equal to 20. For this set of parameters the MPC fluid yields a dynamic viscosity, $\eta = 16.66 k_BT\,\tau a^{-3}$. In our simulations, the colloids have a radius $R = 2.75a$, a spring constant of $K = 10^4 k_BT/a^2$ is chosen to hold together the relative distance between the C_{60} constituent point particles and a mass $M = 10m$ is associated to them. The latter assures adequate fluid-colloid coupling for the correct hydrodynamic behavior. The free diffusion constant of a passive colloid when embedded in a three dimensional fluid and in the infinite dilute limit is measured to be $D_0 = 1.21 \times 10^{-2} a^2/\tau$, while the rotational diffusion constant is $D_R = 1.2 \times 10^{-3}\tau^{-1}$. This is consistent with the Stokes relation $D_R = 3D_0/(2R)^2$. We characterize the activity in terms of the dimensionless Péclet number, $Pe = (2u_0R)/D_0$. Different values of Pe are obtained by varying the propulsion speed for a fixed diffusion. In all our simulations, we consider colloidal swimmers embedded in a three-dimensional fluid, yet their translation and rotation dynamics is constrained in a two-dimensional plane.

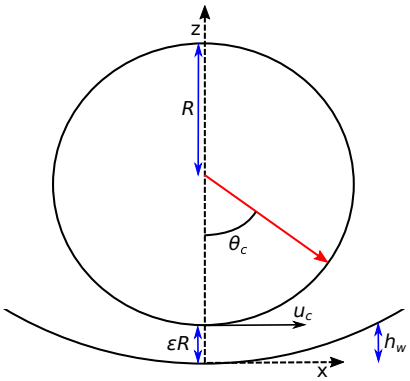

Fig. 1 Reference sketch of an active colloid of radius, R, at a distance εR from a curved surface. The red arrow indicates the colloid propelling axis, which forms an inclination angle θ_c with the surface normal. The direction of the slip velocity of the closest point, u_c, is also shown. The y-axis is into the page.

3 Theoretical description

The near-field hydrodynamic behavior of an active colloidal swimmer near a wall has been studied using lubrication theory[35,36,51]. It is assumed that the closest distance (gap) between the colloidal surface and the wall is significantly smaller than the radius of the colloid, and the fluid flow is dominated by the surface slip velocity of the closest point to the wall. Here, we generalize those results to include a wall with two possible radii of curvature; one that is co-planar with the two-dimensional space, the X-Z plane, where the colloid moves, and the other that is perpendicular to it. Specifically, the wall surface in the vicinity of the contact point can be approximated as

$$h_w(x,y) = \left(\frac{R}{R_x}\right)\frac{x^2}{2} + \left(\frac{R}{R_y}\right)\frac{y^2}{2}, \quad (9)$$

where R_x and R_y are the two surface radii of curvature, and the origin of the coordinate system is placed immediately below the contact point (see Fig. 1). In the above expression, the lengths in the $X-Y$ plane, which is the plane of the dominant flow for the lubrication problem, are rescaled by $\sqrt{\varepsilon}R$ and the lengths in the Z-direction are scaled by εR. Here, ε is the ratio between the colloidal-surface gap from the wall and the colloid radius, with $\varepsilon \ll 1$. The different limits of $\alpha_x = (R/R_x)$ and $\alpha_y = (R/R_y)$ correspond to the following surface geometries

- flat surface: $\alpha_x \to 0$ and $\alpha_y \to 0$
- spherical surface: $\alpha_x = \alpha_y$
- cylindrical surface: $\alpha_x \to 0$ or $\alpha_y \to 0$
- ellipsoidal surface: $\alpha_x\alpha_y > 0$
- toroidal surface: $\alpha_x\alpha_y < 0$.

Using the general form for the wall surface given in Eq. 9 for the boundary conditions, the corresponding leading order contribution to the lubrication force and torque parallel to the wall are given by

$$F_x = \frac{4\pi\eta R u_c}{\sqrt{(1-\alpha_x)(1-\alpha_y)}}\frac{(1-3\alpha_x-\alpha_y)}{(5-3\alpha_x-2\alpha_y)}\ln\varepsilon, \quad (10)$$

$$T_y = \frac{4\pi\eta R^2 u_c}{\sqrt{(1-\alpha_x)(1-\alpha_y)}}\frac{(4-3\alpha_x-\alpha_y)}{(5-3\alpha_x-2\alpha_y)}\ln\varepsilon. \quad (11)$$

Here, u_c is the colloid-surface slip velocity at the point of closest approach. These expressions are consistent with the results of ref.[51] in the limit of a spherical surface and for a flat surface as in ref.[35]. The near-field results are the significant contributions for colloids that are almost at contact with the surface. For colloids that are close (but not in contact) to the surface a perturbation due to the back of the colloid (outer surface) becomes important and can be approximated by a far-field contribution[37]. Indeed, it was recently reported[35] that the leading order contribution to the velocity comes from the outer region.

The fluid flow in the far-field of a squirmer is well established in the literature[34,35]. A similar approximate expression for the far-field of the active Janus colloid near a no-slip flat surface can be derived via Lorentz reciprocal theorem[52,53]. In our case, the auxiliary problem for the reciprocal theorem is the Stokes drag on a passive sphere with translational and rotational motion near a surface, for which the flow field in terms of fundamental flow singularities computed via the method of images is very well known[52,54]. From the reciprocal theorem, the leading-order contribution to the motion of an active Janus colloid due to its interaction with a no-slip flat-wall in the far-field is given by

$$v_f = u_0\sin\theta_c + \frac{9}{64}\left(\frac{R}{h}\right)^2 u_0\beta\sin 2\theta_c + \mathcal{O}(h^{-3}), \quad (12)$$

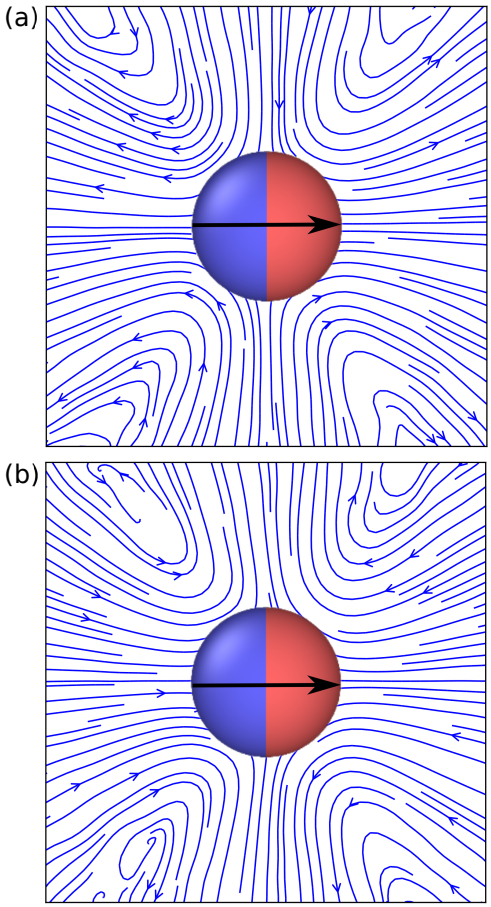

Fig. 2 Numerically extracted bulk flow fields of the surrounding fluid around a (a) strong-pusher ($\beta = -5.25$), (b) strong-puller ($\beta = 5.25$). In both cases we considered a standard squirmer-slip from the surface. The black arrow indicates the direction of propulsion.

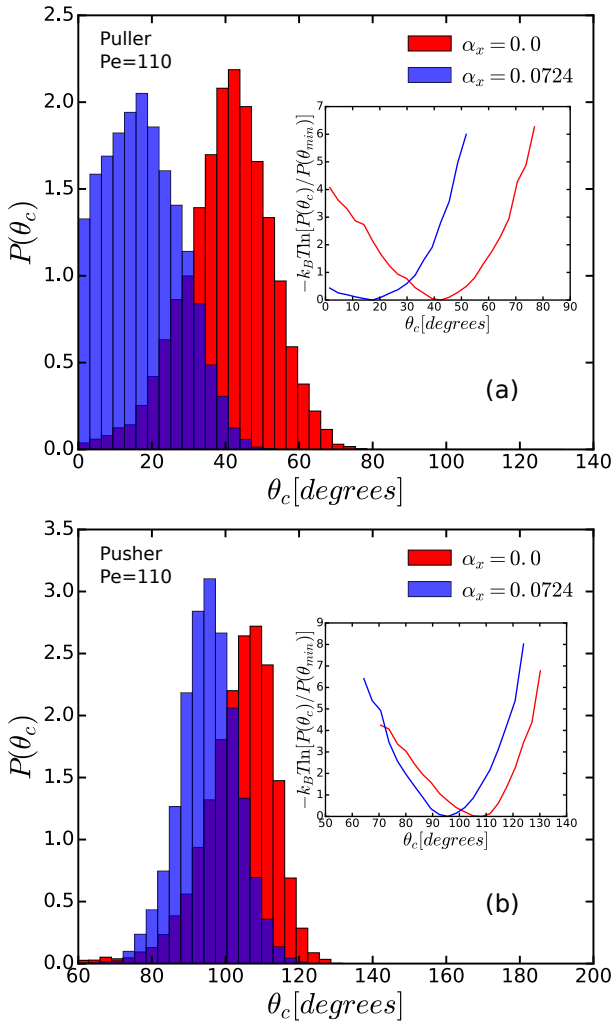

Fig. 3 CYLINDRICAL SURFACE: Distribution of the inclination angle, θ_c, of a squirmer near surfaces with in-plane curvature $\alpha_x = R/R_x = 0$ (red) and $\alpha_x = R/R_x = 0.0724$ (blue) for (a) $Pe = 110$, $\beta = 5.25$ (puller) and (b) $Pe = 110$, $\beta = -5.25$ (pusher). The insets show the relative thermal stability of the average angle θ_{min} selected by the swimmers.

$$R\Omega_f = \frac{9}{128}\left(\frac{R}{h}\right)^3 u_0\beta\sin 2\theta_c + \mathcal{O}(h^{-4}). \quad (13)$$

Here, v_f and Ω_f are the colloid translational velocity and angular velocity parallel to the wall, θ_c is the inclination angle of the colloid orientation with the wall normal, h is the distance from the center of the colloid to the no-slip wall. These expressions refer to the case where $h \gg R$. When $h \approx R$, the outer contribution to the translational and angular velocity of the active Janus colloid near a non-flat boundary can thus be approximated, by analogy with the Faxen's law for the far-field contribution of the squirmer model, as

$$v_{out} = \lambda_1\left(R_x,R_y\right)u_0\sin\theta_c + \lambda_2\left(R_x,R_y\right)u_0\beta\sin 2\theta_c, \quad (14)$$

$$R\Omega_{out} = \lambda_3\left(R_x,R_y\right)u_0\sin\theta_c + \lambda_4\left(R_x,R_y\right)u_0\beta\sin 2\theta_c. \quad (15)$$

Here, $\lambda_1(R_x,R_y)$, $\lambda_2(R_x,R_y)$, $\lambda_3(R_x,R_y)$ and $\lambda_4(R_x,R_y)$ are coefficients expected to be dependent on the local curvature of the wall.

The parallel translational speed of the active colloid can be estimated by combining the force contribution from the lubrication region and that from the outer region. Thus, the force-free condition (no external forces) on a colloid moving with speed v_x in the x-direction (parallel to the surface) gives

$$6\pi\eta R(v_{out} - v_x) + \frac{4\pi\eta R\ln\varepsilon(u_c + v_x)}{\sqrt{(1-\alpha_x)(1-\alpha_y)}}\frac{(1-3\alpha_x-\alpha_y)}{(5-3\alpha_x-2\alpha_y)} = 0. \quad (16)$$

If the outer contribution v_{out} is known, then the above expression can be used to extract the speed v_x. Similarly, the torque-free condition yields

$$8\pi\eta R^3\Omega_{out} + \frac{4\pi\eta R^2\ln\varepsilon(u_c + v_x)}{\sqrt{(1-\alpha_x)(1-\alpha_y)}}\frac{(4-3\alpha_x-\alpha_y)}{(5-3\alpha_x-2\alpha_y)} = 0, \quad (17)$$

from which one can extract the orientation of the particle with respect to the normal to the surface, provided an estimate of Ω_{out} is available. Although there is not a simple way of estimating the λ coefficients in Eqs. 14 and15, these parameters can be directly extracted from numerical simulations.

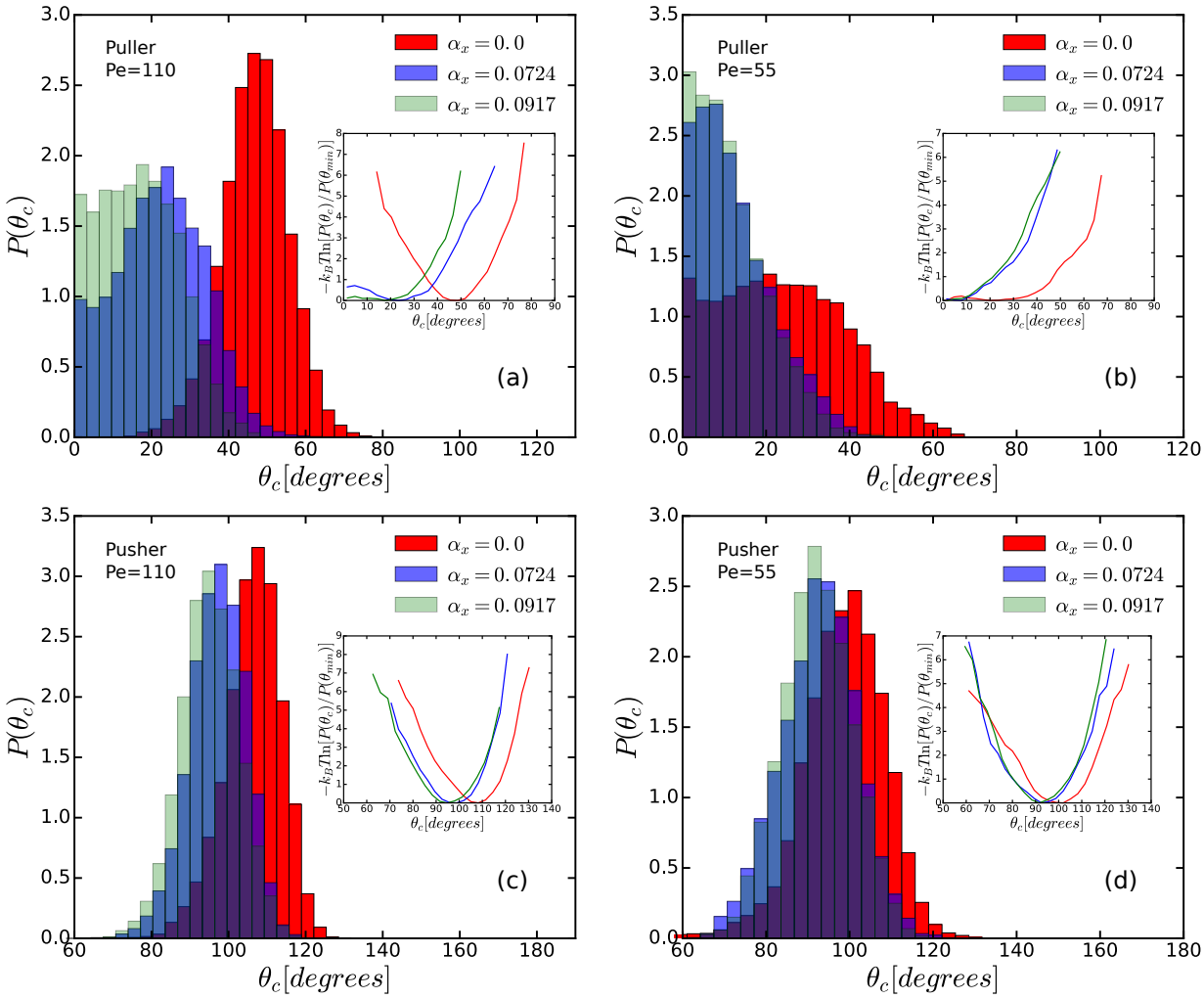

Fig. 4 CYLINDRICAL SURFACE: Distribution of the inclination angle of a Janus colloid near surfaces with curvature $\alpha_x = R/R_x = 0$ (red), 0.0724 (blue), 0.0917 (green) for (a) $Pe = 110$, $\beta = 5.25$ (puller), (b) $Pe = 55$, $\beta = 5.25$ (puller), (c) $Pe = 110$, $\beta = -5.25$ (pusher) and (d) $Pe = 55$, $\beta = 5.25$ (pusher). The insets show the relative thermal stability of the angle θ_{min} selected by the swimmers.

4 Results

We begin our numerical analysis by checking that our colloidal swimmer model reproduces the expected bulk properties of a single colloidal particle of comparable size, i.e. we measured the mean-square-displacement (MSD) and orientational correlation over time. While the orientational correlation is independent of the strength of the active force and the type of the swimmer, as the thermal fluctuation are solely responsible for the rotational diffusion in the infinite dilute limit, the MSD shows the expected u_0^2 dependence in the diffusive regime. Figure 2 shows the fluid flow-field for a puller and a pusher-type colloidal swimmer with a surface-slip described by the standard squirmer model. These patterns are fully consistent with those previously reported in the literature[37,55]. Next, we consider the behavior of our colloidal particle near a smooth wall.

4.1 Swimming modes

As discussed earlier, hydrodynamic torques reorient an active swimmer when it approaches a no-slip wall and depending on the type of swimmer different modes of locomotion, e.g. lateral sliding, scattering and hovering, are observed[35,37]. More specifically, while strong pushers tend to move parallel to the surface and strong pullers slide laterally with the propelling axes facing the surface, neutral, weak pullers and weak pushers are generally able to escape the surface by reorienting their propelling axis.

In our simulations, for both the squirmer and the Janus colloid, we observe a similar kind of locomotion near a flat no-slip surface. We considered five distinct cases characterized by different values of the parameter β which determines the type of swimmer. β = -5.25 (strong pusher), β = -1.5 (weak pusher), β = 0 (neutral), β = 1.5 (weak puller), β = 5.25 (strong puller). As expected, for both squirmers and Janus colloids when $|\beta| \leq = 1.5$ the particle tends to leave the surface some time after making contact. The results showing the probability distributions of the orientational angles, $P(\theta_c)$, for strong squirmers at $Pe = 110$ are shown in Fig. 3

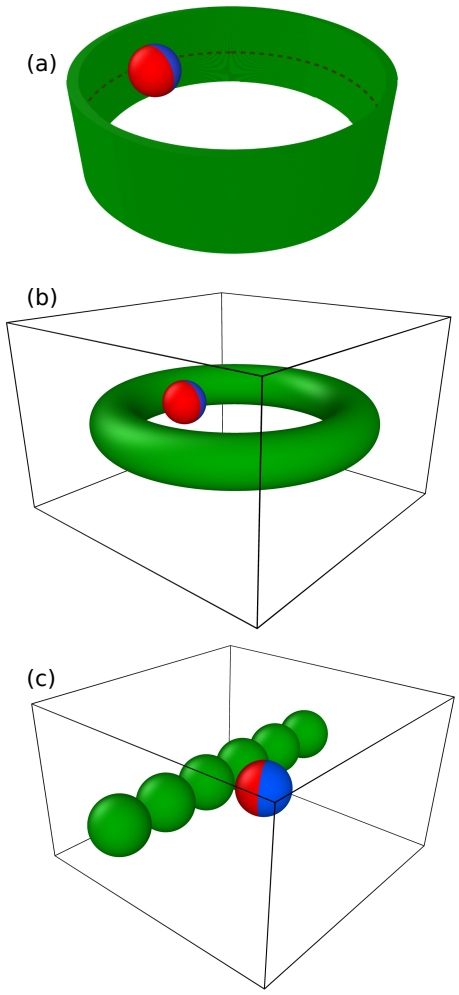

Fig. 5 Sketches of the surfaces considered in the simulations. (a) Infinitely long cylinder with the axis perpendicular to the plane of motion, and fully containing the fluid. (b) Finite sized torus with its the axis perpendicular to the plane of motion, and surrounded by an unbounded fluid. (c) A linear string of colloidal particles lying in the plane of motion, and surrounded by an unbounded fluid.

(case $\alpha_x = 0$), the same data for the Janus colloid are shown in Fig. 4(a),(c)). Strong pullers pick up an angle $\theta_{min} \approx 40^\circ$ when propelled according to the squirmer-slip and an angle $\theta_{min} \approx 45^\circ$ when propelled with the Janus-like slip velocity at $Pe = 110$. Since the system is at steady states, the deviations from the equilibrium angle are due to thermal fluctuations. It is therefore reasonable to interpret $-k_B T \ln[P(\theta_c)]$ as an effective free energy providing information about the thermal stability of that hydrodynamically selected angle θ_{min}. The insets of the figures, therefore, also show how $-k_B T \ln[P(\theta_c)/P(\theta_{min})]$ depends on θ_c, and indicate that several $k_B T$s are required to either change the direction of motion of the particle on the surface by selecting the symmetric point at $-\theta_{min}$, or move away from the surface by reaching an angle larger than 90°. Either cases are therefore very unlikely to occur spontaneously. Similarly, a strong pusher picks up an orientation angle $\theta_{min} \approx 106^\circ$ against the surface normal for both the squirmer and the Janus colloid slip type. Figures 3(b) and 4(c) show the results of this analysis for the two cases at $Pe = 110$. The swimming

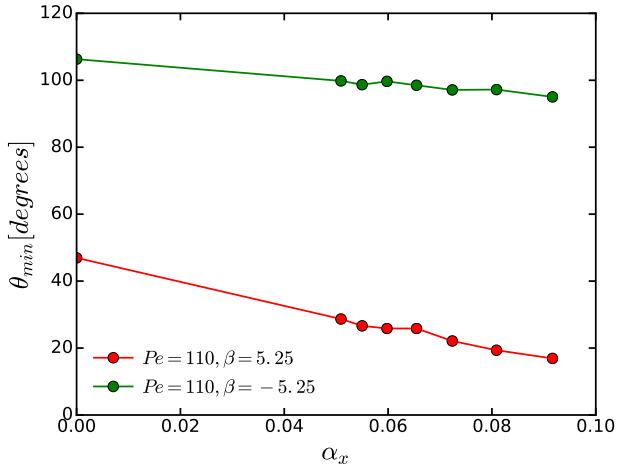

Fig. 6 CYLINDRICAL SURFACE: The average inclination angle of a Janus colloid near a no-slip surface as a function of the in-plane surface curvature α_x, for $Pe = 110$, $\beta = 5.25$ (puller), and $Pe = 110$, $\beta = -5.25$ (pusher).

modes of both models are indeed expected to be qualitatively similar near a flat no-slip wall[37]. A direct comparison of our results for the squirmer model with those of Ishimoto et. al.[56] gives a reasonable agreement of the steady state angle, θ_{min}, for pushers, but there is a notable difference for pullers. The reason is that our ε for pushers matches that of Ishimoto et. al., however, our estimate of the same parameter for pullers is a bit different. As the lubrication interaction is the dominant contribution in selecting the steady state angle, a small change in ε can lead to significant changes in θ_{min}.

It is important to stress that the theoretical description of the system discussed in the previous section ignores the role of thermal fluctuations. Solving Eq. 17 for the rotational dynamics predicts an inclination angle θ_{min} that is independent of the Péclet number. We therefore performed simulations also at a different Péclet number, $Pe = 55$, yet with the same values of β. Our numerical results for the Janus colloid are shown in Fig. 4, and indicate that upon decreasing Pe the inclination angle of a strong puller not only acquires a significantly broader distribution with an almost flat free energy barrier around $\theta_c = 0$ (Fig. 4(b)), but also a smaller value of θ_{min}. In other words, thermal fluctuations easily deviate the colloid orientation for relatively lower activity[57] and makes it easy for the particle to invert direction of motion on the surface. Upon increasing Pe to values larger than 110 we observe only a slight increase of θ_{min} followed by a narrowing of the distribution (data not shown). This is likely due to the dependence of the re-scaled gap distance ε with the Péclet number. Our data does indeed indicate that ε decreases when increasing Pe. A similar behavior is observed for pushers (Fig. 4(c),(d)), however, the overall perturbation due to thermal fluctuations is less dramatic, and unlike the case of pullers, we never observe pushers invert their motion along the surface (at least for the Péclet numbers considered in this study).

Next, we examine the effect of the wall curvature on the motion of a strong puller and pusher. For this we consider a colloid inside a cylinder oriented with its axis parallel to the normal to

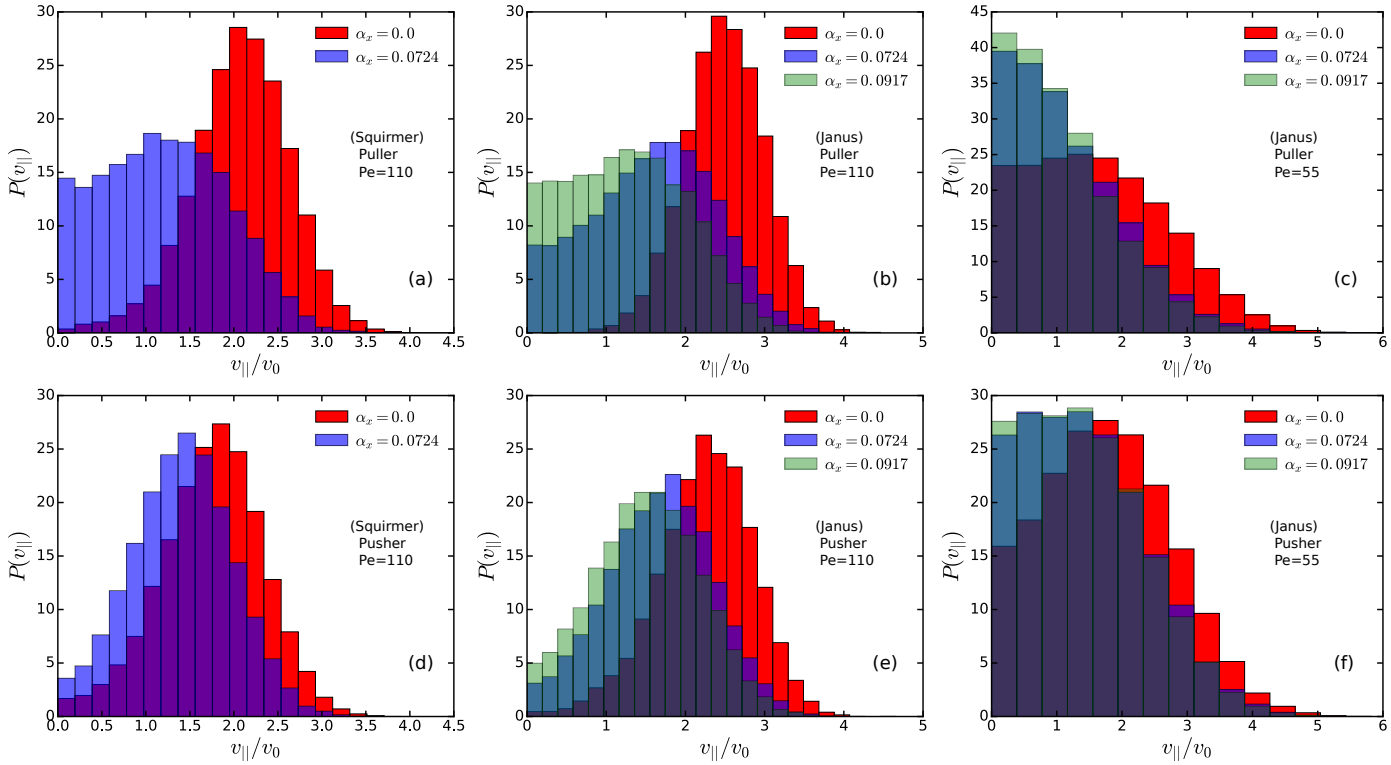

Fig. 7 CYLINDRICAL SURFACE: Distribution of the speed parallel to the surface, $v_{||}$, for an active colloid. The top row is for pullers and the bottom one for pushers. Cases (a) and (d) refer to $Pe = 110$ for a standard squirmer, cases (b) and (d) refer to $Pe = 110$ for a Janus colloid, finally cases (c) and (f) refer to $Pe = 55$ for a Janus colloid. The different colors indicate the various wall curvatures.

the plane of motion of the colloid, see Fig. 5(a). In this study, we only select cylinder radii that are at least ten times larger than the colloidal radius, so that the effect of the confined fluid on the colloidal motion is negligible. As observed in Fig. 3(a) and Fig. 4(a), the distinct peak in the incident angle distribution of a puller at relatively higher Péclet number ($Pe = 110$) shifts to smaller values upon increasing the wall curvature. Furthermore, the angular distribution becomes broader. For instance, already for $\alpha_x \simeq 0.1$ the angular probability for the Janus colloid presents an almost flat profile for any value smaller than θ_{min}. This indicates that the particle can easily switch direction of motion along the surface even for this large Péclet numbers. When considering the pusher, the perturbation of the curvature on the incident angle presents overall a similar trend, yet to a much smaller extent, see Fig. 3(b) and Fig. 4(c). Figures 4(b) and 4(d) show the same analysis for a smaller Péclet number, $Pe = 55$ for the Janus colloid. Even in this case, where thermal fluctuations dominate, change in the angle distribution can be clearly observed as the wall-curvature increases for both strong puller and pusher.

It is worth mentioning that we also performed simulations with weak Janus colloids. Unfortunately, given the relatively short time spent by the particles on the surface, it is hard to obtain accurate distributions for weak Janus swimmers. For completeness, we added the relevant distributions in the supplementary material. Overall, for flat surfaces we observe a similar behavior established for their strong counterparts, however the curvature has a more dramatic impact on the inclination angle. See SFig. 1 and SFig. 2 in the supplementary information.

Back to the case of strong Janus swimmers, using Eq. 17 and our numerical simulations, a rough estimate of the contribution to the rotational motion from the outer region of the colloid away form the wall is achieved. In Fig. 6, we measure the average angle of a Janus colloid at various wall curvatures, and fit the data to extract the λ parameters in Eq. 15. We obtain

$$R\Omega_{out} = -\frac{0.4245}{(1-2.095\alpha_x)} u_0 \beta \sin(2\theta_{min}). \tag{18}$$

We now turn our attention to the particle speed parallel to the surface. Enhanced motion of the swimmers near a no-slip surface, i.e. an increase in the swimming speed near the surface compared to their bulk speed, has been observed in theoretical studies [35,37]. Even in experiments a speed up of the velocity of active Janus colloids near an air-water interface has been reported [58]. This can be understood by considering that both pushers and pullers are orientated near the wall in such a way that the fluid flow due to the colloidal surface-slip near the contact point is against the wall. As a result, they acquire a boost in speed due to hydrodynamic reflection (see Fig. 8(a) and 8(c)), as evident from the lubrication expression for the force Eq. 10. Our results are consistent with these observations as shown in Figure 7 that plots the swimming speed parallel to the surface also as a function of surface curvature. The enhancement of the motion near a flat-surface is significant for the strong pushers and pullers with a speed of $v_{||} \geq 2u_0$ for a standard squirmer, as well as for the Janus colloid. However,

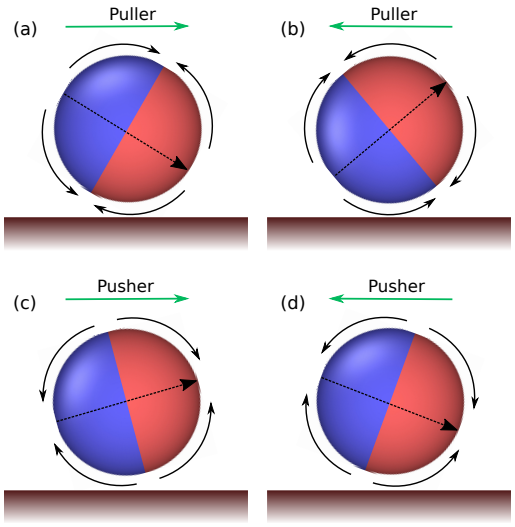

Fig. 8 Schematic of the direction of motion (denoted by the green arrow) of an active Janus colloid depending on its orientation (as denoted by dashed arrows) near a no-slip boundary. (a) and (b) show the motion of pullers. (c) and (d) show the motion of pushers. The solid black arrows indicate the fluid flow direction close to colloid surface.

a notable change in the speed distribution with a reduction in the average speed can be observed for strong pushers-pullers as the wall curvature increases. The speed distributions follow the same trend with the curvature and Péclet number as the ones observed for the angular distributions of the incident angle discussed in Fig. 3 and 4.

In general, one should expect that when a pusher or a puller are aligned in opposite direction with respect to the spontaneous orientation they acquire when near a surface, they should experience a hydrodynamic reflection against the direction of their orientation as sketched in Figs. 8(b) and 8(d). Whenever the strength of the reflections is larger than the swimmer forward momentum, the active colloid moves backwards. This phenomenon has recently been observed for pushers having their axis of propulsion pointing in the direction of the surface (rather than away from it)[38,41]. We observe this backward motion for a pusher-type Janus colloid when a bias potential that forces the self-propelling angle to point towards the surface while simultaneously keeping the particle near the surface is introduced. Interestingly, this behavior is not exclusive to pushers. In fact, we also observe it for the pullers when they are forced to orient away from the surface. The translational velocity of a Janus colloid moving parallel to the wall, $v_{||}$, as a function of its inclination angle θ_c is shown in Fig. 9 for flat wall ($\alpha_x = 0$), and for a curved one with $\alpha_x = 0.0724$. These data were obtained adding a harmonic angular bias to the direction of the propelling axis to force it to point to the desired angles which wouldn't otherwise spontaneously be sampled. Plugging Eq. 14 into Eq. 16 one obtains an expression for $v_{||}$ (labeled as v_x in the theoretical description) in terms of the unknown curvature-dependent lambda coefficients. We fit that functional form to the numerical data for $v_{||}$, and find the expression for the swimming speed near a no-slip surface to

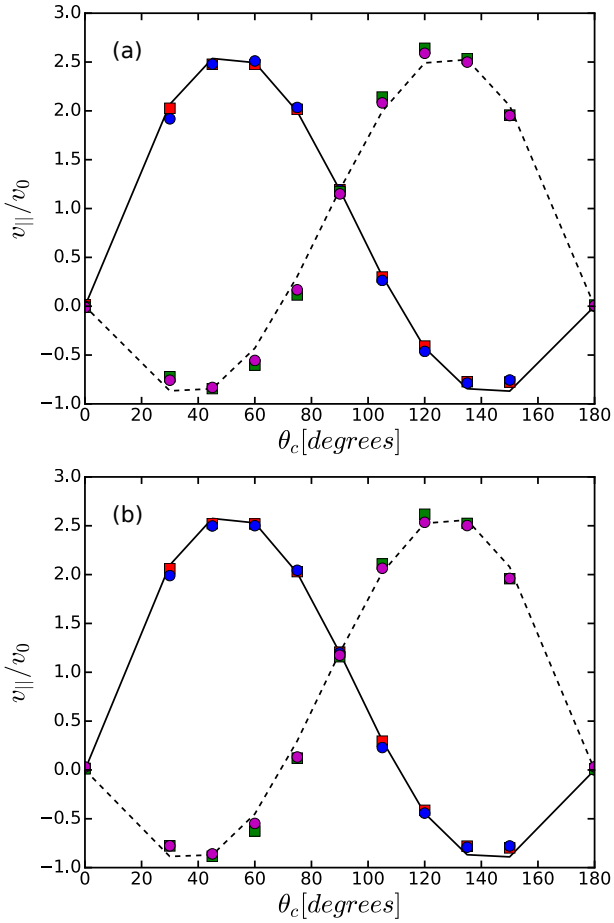

Fig. 9 The magnitude of the velocity of Janus colloids moving parallel to the wall normalized by their bulk velocity as a function of the inclination angle θ_c. Data for curvature $\alpha_x = 0$ are shown in (a). Data for $\alpha_x = 0.0724$ are shown in (b). The data corresponding to $Pe = 110, \beta = 5.25$ are shown with red squares, those for $Pe = 55, \beta = 5.25$ with blue circles, those for $Pe = 110, \beta = -5.25$ with green squares, and those for $Pe = 55, \beta = -5.25$ with magenta circles. The solid and dashed lines are fits for pullers and pushers respectively using Eq. 19.

be well described by the following function

$$\frac{v_{||}}{u_0} = \frac{1}{(1-(2/3)\mu\ln\varepsilon)}\left[\left(\frac{1.38}{(1-1.32\alpha_x)}\frac{9}{64} - \frac{1}{2}\mu\ln\varepsilon\right)\beta\sin 2\theta_{min} + \left(\frac{1.1}{(1-0.254\alpha_x)} - \mu\ln\varepsilon\right)\sin\theta_{min}\right], \tag{19}$$

where $\mu = (1-3\alpha_x)/[\sqrt{1-\alpha_x}(5-3\alpha_x)]$. Here, following the approach in ref.[37], we have considered an approximate continuous form of the surface slip velocity that only includes the first two terms of the Legendre polynomial expansion of Eq. 6. This continuous form does indeed give an accurate dependence of $v_{||}$ on u_0 and β.

Using the expression in Eq. 19, we can predict the onset angle for the backward motion for both pullers and pushers. Notice, however, that such backward motion is only possible in the presence of some sort of biasing potential, for instance a magnetic

field. Furthermore, plugging the expression for $v_{||}$ (Eq. 19) and that for Ω_{out} (Eq. 18) into Eq. 17, one can predict the orientation angle at different curvatures for any type of Janus colloidal swimmer.

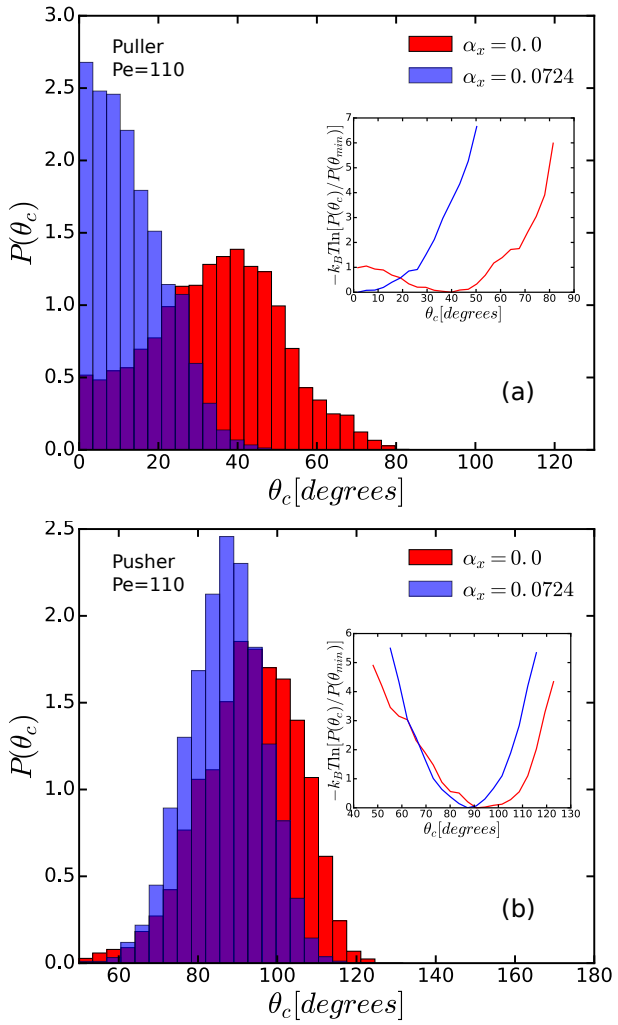

Fig. 10 TOROIDAL SURFACE: Distribution of the inclination angle, θ_c, of (a) Janus puller with $Pe = 110$, $\beta = 5.25$, and (b) Janus pusher with $Pe = 110$, $\beta = -5.25$ near no-slip toroidal surfaces. The surface curvature perpendicular to the plane of motion is set in both cases to $\alpha_y = -1$. The data in red correspond to an in-plane curvature of $\alpha_x = 0$, those in blue to $\alpha_x = 0.0724$. The insets show the relative thermal stability of the angle θ_{min} selected by the swimmers.

For completeness, we also considered the behavior of a strong pusher and puller, $\beta = \pm 5.25$ at $Pe = 110$, near a smooth toroiodal wall. Unlike the previous cases, where the wall is infinite along the direction perpendicular to the plane of colloidal motion, now the wall curves onto itself to form a finite-sized object, and the fluid is not longer fully confined by the wall (see Fig. 5(b)). To be specific, we fix $\alpha_y = R/R_y = -1$, so that the difference between the outer and inner radius of the torus equals the diameter of the particle, and we consider two different values of α_x: $\alpha_x = 0$ and $\alpha_x = 0.0724$. In general, the particle outer region hydrodynamic contributions to the force and torque would also include additional terms dependent on the second radius of curvature, and

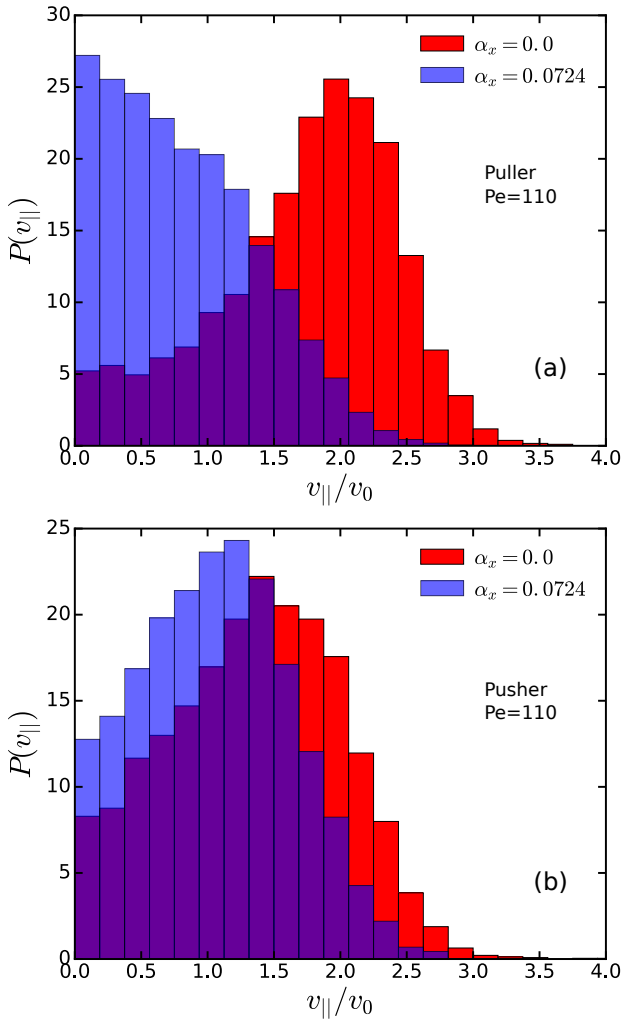

Fig. 11 TOROIDAL SURFACE: Distribution of the speed parallel to the toroidal wall for (a) Janus puller with $Pe = 110$, $\beta = 5.25$, and (b) Janus pusher with $Pe = 110$, $\beta = -5.25$. In both cases, the wall curvature perpendicular to the plane of motion is $\alpha_y = -1$. The data in red correspond to an in-plane curvature of $\alpha_x = 0$, those in blue to $\alpha_x = 0.0724$.

can be extracted following the strategy previously discussed. We will not do that here, and we limit our discussion to the behavior of the orientation angle for the two values of α_x.

As expected from the theory, when compared to the earlier results with a single radius of curvature in the plane of motion, the lubrication contribution to the forces and torques is altered by the presence of a second curvature. For both pullers and pushers, the inclination angle adjusts accordingly and we observe a more relevant role of thermal fluctuations as visible from the significantly broader distributions of the orientational angle. Typically, we observe smaller values of θ_{min} for a fix value of α_x upon introducing the second radius of curvature R_y. This trend is more dramatic when the in-plane curvature α_x is larger than zero. The same trends holds true for the velocity distribution along the wall as can be seen in Fig. 11. The reduction in velocity suggests that the leading hydrodynamic contribution to $v_{||}$, which as discussed earlier is due to the outer region of the particle, decreases upon

increasing α_y.

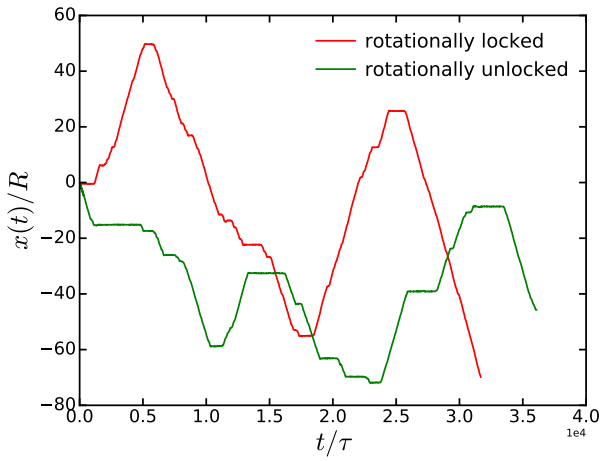

Fig. 12 Trajectories of a Janus puller in the lateral direction of a surface made of colloidal particles. The data in green refer to the case where the colloids are free to rotate, those in red refer to colloids that are rotationally locked-in.

4.2 Colloidal walls

In this final section, we briefly discuss the behavior of a Janus swimmer near a colloidal crystalline interface built by placing particles, having the same diameter as the swimmer, in linear formation and at a kissing distance from each other, see Fig. 5(c). We consider two distinct cases: one where the colloids forming the boundary are translationally locked in place, but are free to rotate, and one where also the rotational degrees of freedom are forbidden. The first case mimics the presence of a crystal formed by colloidal particles interacting via a strong isotropic potential, whereas the second scenario corresponds to the case where the colloids are held together by strong directional interactions. For both scenarios, we only consider the limit where the strength of the active forces is small enough that no disruption of the order/position of the colloids on the surface is expected.

For both colloidal surfaces, we find that a strong pusher, $\beta = -5.25$ and Péclet number $Pe = 110$, upon approaching the surface tilts its axis of propulsion to form an angle of roughly 90 degrees, and moves near it until it finally leaves it. The main difference between the two surfaces is that the residence time of the swimmer near the rotationally frozen colloids is much longer than that near freely rotating colloids. Furthermore, in the latter case, the momentum due to the slip velocity of the swimmer is also transferred to the colloids in contact with it which begin to rotate accordingly. The net result is that the swimmer moves at a relatively lower speed along the surface and feels an overall weaker attraction to it.

The behavior is rather different when considering strong Janus pullers. In this case, when the rotational degrees of freedom of the colloids are locked in, the swimmer can become locally trapped when it stacks between two passive colloids. In fact, when the swimmer axis points towards the normal to the surface in that configuration, the lubrication force from the nearest left and right colloids is perfectly balanced and no net motion can occur. Only when thermal fluctuations drive the swimmer out of that configuration, a net (lateral) sliding motion on the surface can be achieved. This results in a run-and-tumble-like motion along the surface. Allowing the colloids on the surface to freely rotate has the main effect of increasing the time a Janus swimmer remains locked-in when stacked between two colloids, and shortening the average length of the directed motion along the surface in between two successive trapping events. Apart from that, the swimmers are moving at roughly the same speed, as evident from the slopes in Fig. 12 which shows typical time trajectories of Janus swimmers near these two kinds of surfaces.

5 Conclusions

In this paper, we presented a combination of theoretical calculations and numerical simulations to understand the motion of different kinds of colloidal swimmers adjacent to various surfaces. Our numerical calculations include hydrodynamic interactions as well as thermal fluctuations, and can be used to extract a set of parameters that can be fed to our theoretical expressions to estimate the complex dependence of the hydrodynamics contribution for the outer region of the colloid on the curvature of a no-slip surface. These results can be used to predict the inclination angle and the parallel speed of an active Janus colloid. Moreover, they shed light on the origin of the backward motion of an active colloid near a surface observed when its axis of propulsion is tilted beyond an onset value. We show that such a backward motion is feasible for both pushers and pullers when they orient contrary to their natural inclination near a no-slip surface.

Overall, we find that both thermal fluctuations and the local curvature of the surface have a significant effect on the swimming modes of the colloidal swimmers near the surface. We detail how both effects alter the average tilt angles and surface velocities acquired by the swimmers with respect to the case of an infinite flat wall, and show how their distributions change with these parameters.

Although our theoretical description should hold for any wall geometry, in this study, we presented numerical simulations for flat, cylindrical, and toroidal geometries for the wall. We have not considered the case of a spherical wall because in this case it is hard to numerically disentangle the effect of the wall near the swimmer from that of the confined fluid away from it on the tilt angle and parallel velocity of the swimmer on the surface. We should also mention that we performed a few simulations considering convex surfaces, i.e. a Janus active colloid near a frozen, larger spherical colloid. In this case we observe trapping of the Janus swimmer on the colloidal surface for both pushers and pullers, but overall, it is easier to trap pullers rather than pushers. This is consistent with the results reported in reference[39].

Most of our results has been obtained for swimmers with $|\beta| = 5.25$, this is because, as discussed in the paper, the hydrodynamic attraction for very weak swimmers, $|\beta| = 1.5$, is rather weak, and thermal fluctuations are able to easily disrupt their motion and push them away from the surface, nevertheless they show a behavior similar to their stronger counterparts when bound to it. A very recent experimental study, published while finalizing

this paper[59], reported a direct measurement of the flow field around a Pt-PS colloidal swimmer. This was mapped into an effective squirmer-like model. For this specific system it was found $\beta = -2.45$ roughly in the middle of our range. Although it is not clear that a mapping onto a simple squirmer model can always be done accurately, and different active components could have different degrees of strength β, our results suggests that additional interactions, beyond the hydrodynamic ones, between particle and surface would be necessary for weak swimmers to have a significant residence time near a surface.

Finally, we discussed the case of swimmers near the surface of a colloidal crystal, and show how in this case the dynamics of the pullers can be described as a run-and-tumble motion rather then a persistent, unidirectional one. Although, this study is limited to stiff colloidal interfaces whose relative position is unaffected by the active forces, it nonetheless gives useful insight into the behavior of active colloids in passive/active binary mixtures in the limit of strongly attractive passive particles. An extension of this work considering colloidal surfaces held together by explicit interactions competing with the active forces is underway. It is worth pointing out that a system of ABP particles with a short range attraction [60], can be mapped into an effective weak pusher swimmer. This can be argued by looking at the statistics of the clusters during phase separation. Furthermore, using similar arguments it was shown[61] that under certain conditions it is possible to map the behavior of repulsive ABP particles into an effective run-and-tumble system. Unlike these works, the run-and-tumble-like motion developed by our swimmer only occurs for pullers near a corrugated boundary and it emerges from an explicit hydrodynamic trapping and thermal releasing of individual particles from within the interstitial spaces between the colloids. As such, our results do not directly add to the discussion on the effective mapping between the collective behavior of swimmers and run-and-tumble particles while phase separating in the bulk.

Conflicts of interest

There are no conflicts to declare.

Acknowledgements

We thank Roland G. Winkler for insightful discussions. A.C. acknowledges financial support from the National Science Foundation under Grant No. DMR-1703873. We gratefully acknowledge the support of the NVIDIA Corporation for the donation of the Titan V GPU used to carry out this work.

References

1 R. Golestanian, T. Liverpool and A. Ajdari, *New Journal of Physics*, 2007, **9**, 126.
2 J. R. Howse, R. A. Jones, A. J. Ryan, T. Gough, R. Vafabakhsh and R. Golestanian, *Physical review letters*, 2007, **99**, 048102.
3 G. Volpe, I. Buttinoni, D. Vogt, H.-J. Kümmerer and C. Bechinger, *Soft Matter*, 2011, **7**, 8810–8815.
4 M. Mijalkov and G. Volpe, *Soft Matter*, 2013, **9**, 6376–6381.
5 I. Buttinoni, G. Volpe, F. Kümmel, G. Volpe and C. Bechinger, *Journal of Physics: Condensed Matter*, 2012, **24**, 284129.
6 J. Palacci, S. Sacanna, A. P. Steinberg, D. J. Pine and P. M. Chaikin, *Science*, 2013, **339**, 936–940.
7 S. Das, M. Lee Bowers, C. Bakker and A. Cacciuto, *The Journal of chemical physics*, 2019, **150**, 134505.
8 I. Buttinoni, J. Bialké, F. Kümmel, H. Löwen, C. Bechinger and T. Speck, *Physical review letters*, 2013, **110**, 238301.
9 M. E. Cates and J. Tailleur, *Annu. Rev. Condens. Matter Phys.*, 2015, **6**, 219–244.
10 I. Theurkauff, C. Cottin-Bizonne, J. Palacci, C. Ybert and L. Bocquet, *Physical review letters*, 2012, **108**, 268303.
11 J. Elgeti, R. G. Winkler and G. Gompper, *Reports on progress in physics*, 2015, **78**, 056601.
12 K. Schaar, A. Zöttl and H. Stark, *Physical review letters*, 2015, **115**, 038101.
13 M. C. Marchetti, J.-F. Joanny, S. Ramaswamy, T. B. Liverpool, J. Prost, M. Rao and R. A. Simha, *Reviews of Modern Physics*, 2013, **85**, 1143.
14 G.-J. Li and A. M. Ardekani, *Physical Review E*, 2014, **90**, 013010.
15 I. O. Götze and G. Gompper, *Physical Review E*, 2010, **82**, 041921.
16 I. Llopis and I. Pagonabarraga, *EPL (Europhysics Letters)*, 2006, **75**, 999.
17 I. Llopis and I. Pagonabarraga, *Journal of Non-Newtonian Fluid Mechanics*, 2010, **165**, 946–952.
18 J. Blaschke, M. Maurer, K. Menon, A. Zöttl and H. Stark, *Soft Matter*, 2016, **12**, 9821–9831.
19 E. Lauga and T. R. Powers, *Reports on Progress in Physics*, 2009, **72**, 096601.
20 G. Li and J. X. Tang, *Physical review letters*, 2009, **103**, 078101.
21 G. Li, J. Bensson, L. Nisimova, D. Munger, P. Mahautmr, J. X. Tang, M. R. Maxey and Y. V. Brun, *Physical Review E*, 2011, **84**, 041932.
22 J. Hu, A. Wysocki, R. G. Winkler and G. Gompper, *Scientific reports*, 2015, **5**, 9586.
23 A. P. Berke, L. Turner, H. C. Berg and E. Lauga, *Physical Review Letters*, 2008, **101**, 038102.
24 J. Elgeti and G. Gompper, *The European Physical Journal Special Topics*, 2016, **225**, 2333–2352.
25 S. E. Spagnolie, G. R. Moreno-Flores, D. Bartolo and E. Lauga, *Soft Matter*, 2015, **11**, 3396–3411.
26 D. Takagi, J. Palacci, A. B. Braunschweig, M. J. Shelley and J. Zhang, *Soft Matter*, 2014, **10**, 1784–1789.
27 A. T. Brown, I. D. Vladescu, A. Dawson, T. Vissers, J. Schwarz-Linek, J. S. Lintuvuori and W. C. Poon, *Soft Matter*, 2016, **12**, 131–140.
28 S. Das, A. Garg, A. I. Campbell, J. Howse, A. Sen, D. Velegol, R. Golestanian and S. J. Ebbens, *Nature communications*, 2015, **6**, 8999.
29 S. Herminghaus, C. C. Maass, C. Krüger, S. Thutupalli, L. Goehring and C. Bahr, *Soft matter*, 2014, **10**, 7008–7022.
30 W. Uspal, M. N. Popescu, S. Dietrich and M. Tasinkevych, *Soft Matter*, 2015, **11**, 434–438.

31 A. Mozaffari, N. Sharifi-Mood, J. Koplik and C. Maldarelli, *Physics of Fluids*, 2016, **28**, 053107.

32 Y. Ibrahim and T. B. Liverpool, *EPL (Europhysics Letters)*, 2015, **111**, 48008.

33 W. Uspal, M. N. Popescu, S. Dietrich and M. Tasinkevych, *Soft Matter*, 2015, **11**, 6613–6632.

34 S. E. Spagnolie and E. Lauga, *Journal of Fluid Mechanics*, 2012, **700**, 105–147.

35 J. S. Lintuvuori, A. T. Brown, K. Stratford and D. Marenduzzo, *Soft Matter*, 2016, **12**, 7959–7968.

36 T. Ishikawa, M. Simmonds and T. J. Pedley, *Journal of Fluid Mechanics*, 2006, **568**, 119–160.

37 Z. Shen, A. Würger and J. S. Lintuvuori, *The European Physical Journal E*, 2018, **41**, 39.

38 M. Kuron, P. Stärk, C. Holm and J. de Graaf, *Soft Matter*, 2019, **15**, 5908–5920.

39 N. Sharifi-Mood, P. G. Díaz-Hyland and U. M. Córdova-Figueroa, *arXiv preprint arXiv:1710.10578*, 2017.

40 O. Sipos, K. Nagy, R. Di Leonardo and P. Galajda, *Physical review letters*, 2015, **114**, 258104.

41 Z. Shen, A. Würger and J. S. Lintuvuori, *Soft matter*, 2019, **15**, 1508–1521.

42 S. Das, J. Riest, R. G. Winkler, G. Gompper, J. K. Dhont and G. Nägele, *Soft Matter*, 2018, **14**, 92–103.

43 S. Poblete, A. Wysocki, G. Gompper and R. G. Winkler, *Physical Review E*, 2014, **90**, 033314.

44 R. Kapral, *Advances in Chemical Physics*, 2008, **140**, 89.

45 G. Gompper, T. Ihle, D. Kroll and R. Winkler, *Advanced computer simulation approaches for soft matter sciences III*, Springer, 2009, pp. 1–87.

46 T. Ihle and D. M. Kroll, *Physical Review E*, 2003, **67**, 066705.

47 C.-C. Huang, A. Chatterji, G. Sutmann, G. Gompper and R. G. Winkler, *Journal of computational physics*, 2010, **229**, 168–177.

48 C.-C. Huang, A. Varghese, G. Gompper and R. G. Winkler, *Physical Review E*, 2015, **91**, 013310.

49 J. Elgeti and G. Gompper, *EPL (Europhysics Letters)*, 2009, **85**, 38002.

50 A. Zöttl and H. Stark, *Journal of Physics: Condensed Matter*, 2016, **28**, 253001.

51 D. R. Brumley and T. J. Pedley, *Phys. Rev. Fluids*, 2019, **4**, 053102.

52 D. Papavassiliou and G. P. Alexander, *EPL (Europhysics Letters)*, 2015, **110**, 44001.

53 H. A. Stone and A. D. Samuel, *Physical review letters*, 1996, **77**, 4102.

54 J. Blake and A. Chwang, *Journal of Engineering Mathematics*, 1974, **8**, 23–29.

55 M. T. Downton and H. Stark, *Journal of Physics: Condensed Matter*, 2009, **21**, 204101.

56 K. Ishimoto and E. A. Gaffney, *Physical Review E*, 2013, **88**, 062702.

57 F. Rühle, J. Blaschke, J.-T. Kuhr and H. Stark, *New Journal of Physics*, 2018, **20**, 025003.

58 X. Wang, M. In, C. Blanc, M. Nobili and A. Stocco, *Soft Matter*, 2015, **11**, 7376–7384.

59 A. I. Campbell, S. J. Ebbens, P. Illien and R. Golestanian, *Nat. Commun.*, 2019, **10**, 1–8.

60 F. Alarcón, C. Valeriani and I. Pagonabarraga, *Soft matter*, 2017, **13**, 814–826.

61 M. E. Cates and J. Tailleur, *EPL (Europhysics Letters)*, 2013, **101**, 20010.